*J. Fluid Mech.* (1979), *vol.* 91, *part* 2, *pp.* 319–335
*Printed in Great Britain*



# Instabilities of convection rolls in a fluid of moderate Prandtl number

By F. H. BUSSE AND R. M. CLEVER
Institute of Geophysics and Planetary Physics,
University of California, Los Angeles

(Received 3 January 1978)

The instabilities of two-dimensional convection rolls in a horizontal fluid layer heated from below are investigated in the case when the Prandtl number is seven or lower. Two new mechanisms of instability are described theoretically as well as experimentally. The knot instability causes the transition to spoke-pattern convection at higher Rayleigh numbers while the skewed varicose instability accomplishes a change to larger horizontal wavelengths of the convection rolls. Both instabilities disappear in the limits of small and large Prandtl number. Although the experimental methods fail in realizing closely the infinitely conducting boundaries assumed in the theory, the observations agree in all qualitative aspects with the theoretical predictions.

## 1. Introduction

Convection in a layer heated from below has attracted increasing attention in recent years as the simplest hydrodynamical system in which the transition to turbulence can be studied. Because of the horizontal isotropy of the heated layer, a characteristic element of turbulence is seen at the onset of convection. In general, the pattern of convection cells realized exhibits a random orientation on a large scale if the influence of the side walls is sufficiently small and if the initial conditions are not controlled. On a small scale of a few layer depths, convection assumes the form of nearly two-dimensional rolls when the variation of the material properties between top and bottom boundaries is negligible except for the linear dependence of the density of temperature. With increasing Rayleigh number this form of convection changes into various forms of truly three-dimensional forms of convection depending on the Prandtl number of the fluid. In experiments started without controlled initial conditions, these transitions are not clearly exhibited since they tend to occur first in particularly inhomogeneous parts of the convection pattern. For this reason a number of experiments have been carried out with controlled initial conditions (Chen & Whitehead 1968; Busse & Whitehead 1971, 1974; Whitehead & Chan 1976); these experiments emphasized high Prandtl number fluids. In the second part of this paper the results of experiments with fluids of Prandtl number 7 or less will be reported; these results are distinctly different from those for higher Prandtl numbers.

Since patterns of uniform convection rolls can be generated in experiments with controlled initial conditions, observations of instabilities can readily be compared with theoretical predictions. Convection is one of the few cases where transitions from two-dimensional to three-dimensional forms of motion are currently accessible

0022-1120/79/4128-6040 $02.00 

to numerical analysis. The first transition that has been investigated theoretically is the transition to bimodal convection (Busse 1967), which occurs predominantly at high Prandtl numbers. This transition is caused by the instability of the thermal boundary layers in much the same way as the onset of convection corresponds to the instability of the static layer. An entirely different instability occurs at low Prandtl numbers in the form of waves propagating along the convection rolls (Busse 1972). This oscillatory instability is the main cause of the transition to time-dependent convection. A computational program for the investigation of instabilities of convection rolls at arbitrary Prandtl numbers was developed by Clever & Busse (1974); they described results for the instabilities leading to bimodal and oscillatory convection for a number of representative Prandtl numbers. A restricted coverage of the parameter range of potentially unstable disturbances caused two new forms of instability to be overlooked. Both the knot instability and the skewed varicose instability are predominant at Prandtl numbers of order unity. The first part of this paper describes the computational results obtained for these instabilities. The comparison with the experimental observations in the second part of the paper demonstrates agreement between experiment and theory in all basic aspects of the problem.

Since the mathematical analysis of convection rolls and their instabilities has been described in the earlier paper (Clever & Busse 1974, hereafter referred to as I), only a brief outline of the methods of analysis is given in § 2. The notation of I will be used throughout this paper. The numerical results are discussed in § 3. The description of the experimental technique in § 4 is kept relatively short by referring the reader to earlier papers on this subject; § 5 presents the observations. The boundary conditions of the theory cannot be as closely approached as in the case of high Prandtl number fluids owing to experimental limitations, but the discrepancy between experimental and theoretical conditions has only a quantitative influence. The paper concludes with some more general remarks in § 6.

## 2. Mathematical formulation of the problem

### 2.1. *Basic equations*

The theoretical description of convection in a horizontal fluid layer heated from below is based on the Navier–Stokes equations and the heat equation. Using the Oberbeck–Boussinesq approximation, the equations can be written in the non-dimensional form given by expressions (1), (2) and (3) of I. Length, time and temperature are measured in terms of the thickness $h$ of the layer, the thermal time scale $h^2/\kappa$ and $\Delta T/R$, respectively, where $\kappa$ is the thermal diffusivity, $\Delta T$ is the temperature difference between the boundaries and $R$ is the Rayleigh number. For the numerical analysis it is convenient to replace the velocity vector $\mathbf{v}$ by two scalar potentials $\phi$ and $\psi$ according to the general representation for the solenoidal vector field $\mathbf{v}$:

$$\mathbf{v} = \boldsymbol{\delta}\phi + \boldsymbol{\epsilon}\psi,$$

where the operators $\boldsymbol{\delta}$ and $\boldsymbol{\epsilon}$ are defined by

$$\boldsymbol{\delta}\phi = \nabla \times (\nabla \times \boldsymbol{\lambda}\phi), \quad \boldsymbol{\epsilon} = \nabla \times \boldsymbol{\lambda}\psi$$

and where $\boldsymbol{\lambda}$ is the unit vector normal to the layer. By taking the vertical component

of the curl and the curl (curl) of the equation of motion, the equations for $\phi$ and $\psi$ are given by (5) and (6) of I. These equations, together with the equation for the deviation $\theta$ of the temperature from the static distribution [given by (7) of I] describe the problem of convection completely if the boundary conditions are specified. Assuming a Cartesian system of co-ordinates with the $z$ co-ordinate in the direction of $\boldsymbol{\lambda}$, the position of the boundaries is given by $z = \pm\frac{1}{2}$. We shall restrict attention to the case of rigid boundaries with prescribed constant temperatures. Accordingly, the conditions

$$\phi = \partial_z \phi = \psi = \theta = 0 \quad \text{at} \quad z = \pm\tfrac{1}{2} \tag{2.1}$$

are required.

For the investigation of the instabilities of convection rolls, the analysis proceeds in two steps. In the first step, two-dimensional steady solutions are obtained which correspond to the convection rolls observed in the experiments. In the second step, infinitesimal disturbances of arbitrary three-dimensional form are superimposed on the steady solution. If a growing disturbance is found, the roll solution is unstable; if no growing disturbance exists, it is stable. In addition to the Rayleigh number $R$, the Prandtl number $P \equiv \nu/\kappa$ and the wavenumber $\alpha$ of the steady solution are parameters of the problem. The necessity of considering arbitrary infinitesimal disturbances requires the introduction of two additional wavenumber parameters in the stability analysis.

### 2.2. *The steady problem*

Steady solutions of equations (5) and (7) of I depending on $y$ and $z$ only are obtained by a Galerkin technique. $\theta$ and $\phi$ are expanded in terms of orthogonal functions which satisfy the boundary conditions on $\phi$ and $\theta$:

$$\left.\begin{aligned} \phi &= \sum_{\lambda,\nu} a_{\lambda\nu} e^{i\lambda\alpha y} g_\nu(z) \equiv \sum_{\lambda,\nu} a_{\lambda\nu} \phi_{\lambda\nu}, \\ \theta &= \sum_{\lambda,\nu} b_{\lambda\nu} e^{i\lambda\alpha y} f_\nu(z) \equiv \sum_{\lambda,\nu} b_{\lambda\nu} \theta_{\lambda\nu}. \end{aligned}\right\} \tag{2.2}$$

Explicit expressions for $g_\nu(z)$ and $f_\nu(z)$ are given in I. The summation runs through all integers $1 \leqslant \nu \leqslant N$, $-N+\nu \leqslant \lambda \leqslant N-\nu$, where the truncation parameter $N$ is chosen such that the solution changes by a negligible amount when $N$ is replaced by $N+2$. Since we are interested in solutions describing periodic convection rolls, the analysis can be restricted to symmetric solutions with $a_{\lambda\nu} = a_{-\lambda\nu}$ and $b_{\lambda\nu} = b_{-\lambda\nu}$. Another simplification results from the fact that only coefficients with even $\lambda+\nu$ need be considered. The corresponding equations form a closed subset of the general system of equations. Solutions which are not described by this subset, for instance those with two rolls on top of each other, do not exist for Rayleigh numbers less than $1{\cdot}7 \times 10^4$ and cannot be realized physically. For further details on the numerical analysis we refer to I.

### 2.3. *The stability problem*

For the investigation of the stability of the steady two-dimensional solution we superimpose infinitesimal disturbances $\{\tilde{\phi}, \tilde{\psi}, \tilde{\theta}\}$ of arbitrary three-dimensional spatial dependence. Since the equations for $\tilde{\psi}$, $\tilde{\psi}$ and $\tilde{\theta}$ are linear, homogeneous and do not depend explicitly on $x$ and $t$, an exponential dependence on those variables can be assumed. Because the equations are periodic in $y$, application of Floquet's theory shows that the $y$ dependence of disturbances has the form of a periodic function with

the same period as the steady solution multiplied by a factor $\exp(idy)$. Thus the disturbances can be assumed to have the form

$$\left.\begin{aligned}\tilde{\phi} &= [\sum_{\lambda,\nu} \tilde{a}_{\lambda\nu} e^{i\lambda\alpha y} g_\nu(z)]\, e^{i(dy+bx)+\sigma t},\\ \tilde{\psi} &= [\sum_{\lambda,\nu} \tilde{b}_{\lambda\nu} e^{i\lambda\alpha y} f_\nu(z)]\, e^{i(dy+bx)+\sigma t},\\ \tilde{\theta} &= [\sum_{\lambda,\nu} \tilde{c}_{\lambda\nu} e^{i\lambda\alpha y} f_\nu(z)]\, e^{i(dy+bx)+\sigma t}.\end{aligned}\right\} \tag{2.3}$$

The variable $\tilde{\psi}$ has been expanded in the same system of functions $f_\nu(z)$ as $\tilde{\theta}$ since both satisfy the same boundary conditions. Substitution of (2.3) leads to a system of linear homogeneous equations for the coefficients $\tilde{a}_{\lambda\nu}$, $\tilde{b}_{\lambda\nu}$ and $\tilde{c}_{\lambda\nu}$ with $\sigma$ as the eigenvalue. Because the steady solution is represented by coefficients with even $\lambda+\nu$ the system of stability equations separates into two subsystems, one including only coefficients with even $\lambda+\nu$, the other including only coefficients with odd $\lambda+\nu$. Since preliminary computations seemed to indicate that the strongest growing disturbances correspond to $d = 0$ (in the case of finite $b$), $d = 0$ was assumed for most of the computations reported in I. In that case a further symmetry of the stability equations could be used. The revised program on which the present paper is based does not use the additional symmetry.

The results reported in the following section are obtained by first selecting a steady solution characterized by the parameters $R$, $P$ and $\alpha$ and computing the eigenvalues $\sigma$ for disturbances with even $\lambda+\nu$ and for those with odd $\lambda+\nu$ as functions of $b$ and $d$. The eigenvalue $\sigma$ with the maximum real part $\sigma_r$ is then determined for several values of $R$ chosen in such a way that they straddle the critical value at which $\sigma_r$ vanishes. A sufficiently accurate critical value can usually be obtained by interpolation. By determining the critical Rayleigh numbers as a function of $\alpha$, the stability boundaries shown in figures 1 and 2 are obtained. Because of the computational expense, calculations of the stability boundaries as a function of the Prandtl number have been done for only two selected wavenumbers.

## 3. Stability boundaries of convection rolls

### 3.1. *General discussion*

In discussing the results of the stability analysis we consider first the subset of disturbances with odd $\lambda+\nu$. The representative instability of this subset is the cross-roll instability, which is characterized by a finite value of $b$ and vanishing $d$. This instability is present at all Prandtl numbers though its importance diminishes for Prandtl numbers of order unity or less. The name 'cross-roll instability' derives from the fact that disturbances in the form of rolls at right angles to the steady roll pattern grow monotonically. For Rayleigh numbers less than about five times the critical value, the instability occurs when the wavenumber of the steady rolls is either significantly larger or significantly lower than the critical wavenumber $\alpha_c$ and in the course of the instability the original rolls are finally replaced by another nearly two-dimensional roll pattern with a wavenumber close to the critical value. Accordingly the disturbances of maximum growth have a wavenumber $b$ in the neighbourhood of the value 3·117 of $\alpha_c$. At higher Rayleigh numbers $b$ becomes much larger as the

instability assumes a boundary-layer character. In this case the two-dimensional rolls are replaced by the three-dimensional pattern of bimodal convection (Busse & Whitehead 1971). At Prandtl numbers of the order 10 or less, another branch of the cross-roll instability emerges. The growth rate $\sigma$ attains a second maximum at relatively low values of $b$, a possibility that had been overlooked in the previous computations reported in I. Because of the knot-like appearance of the instability in the experimental observations, this particular branch of the cross-roll instability is called the knot instability.

Among the instabilities belonging to the subset of disturbances with even $\lambda+\nu$, the oscillatory instability is the most important because it is responsible for the transition from steady rolls to a time-dependent form of convection. This instability has been investigated in detail in I. The corresponding stability boundary has been recomputed in the course of the present analysis because a more accurate eigenvalue routine became available for the new program. A comparison of figures 1 and 2 with the corresponding figures of I shows that the boundary for the onset of oscillations has changed little.

Second in importance is the skewed varicose instability, which is characterized by a finite ratio of $d/b$. Because of this unusual property and because, like the knot instability, it disappears in the limits of vanishing and infinite Prandtl numbers, where detailed investigations had been made earlier (Busse 1967, 1972), the skewed varicose instability was not included in the analysis of I. Independently of the present analysis, the stability of convection rolls has been investigated by Moir (1976) in connexion with the development of a new numerical method. Moir did computations for isolated values of $\alpha$, $R$ and $P$ and found an instability of the skewed varicose type. But the numerical method did not lend itself to extensive computations and the stability boundary was not determined for this reason. Wherever a comparison is possible, both numerical results are in agreement.

The other instabilities among the disturbances with even $\lambda+\nu$ are the zigzag instability, which is responsible for a small fraction of the boundary of the region of stable rolls, and the Eckhaus instability, which occurs only at low Prandtl numbers. Neither instability is responsible for any transition in the convection pattern as the Rayleigh number is increased. Since they have been discussed in I and since the new analysis has yielded at most some minor modifications of the corresponding stability boundaries, no further discussion is required. Instead attention will be focused on the two new instabilities.

### 3.2. *The knot instability*

The best impression of the knot instability is obtained from the shadowgraph observations, see figures 8 and 10 (plates 2 and 4). The modification of the basic roll pattern produced by this instability is relatively small. The vertical velocity and the associated distortion of the isotherms are increased periodically along the up- and down-going fluid sheets on either side of a convection roll. The strong Prandtl number dependence suggests a dynamic cause for the tendency towards the concentration of up- and down-going motion. The efficient heat transport in the stagnation-point layers at the boundaries generated by concentrated advection of momentum appears to be the main reason for the preference of this kind of motion. The experimental observations indicate that the knot-pattern convection becomes fully developed in the form of spoke-pattern convection at higher Rayleigh numbers.

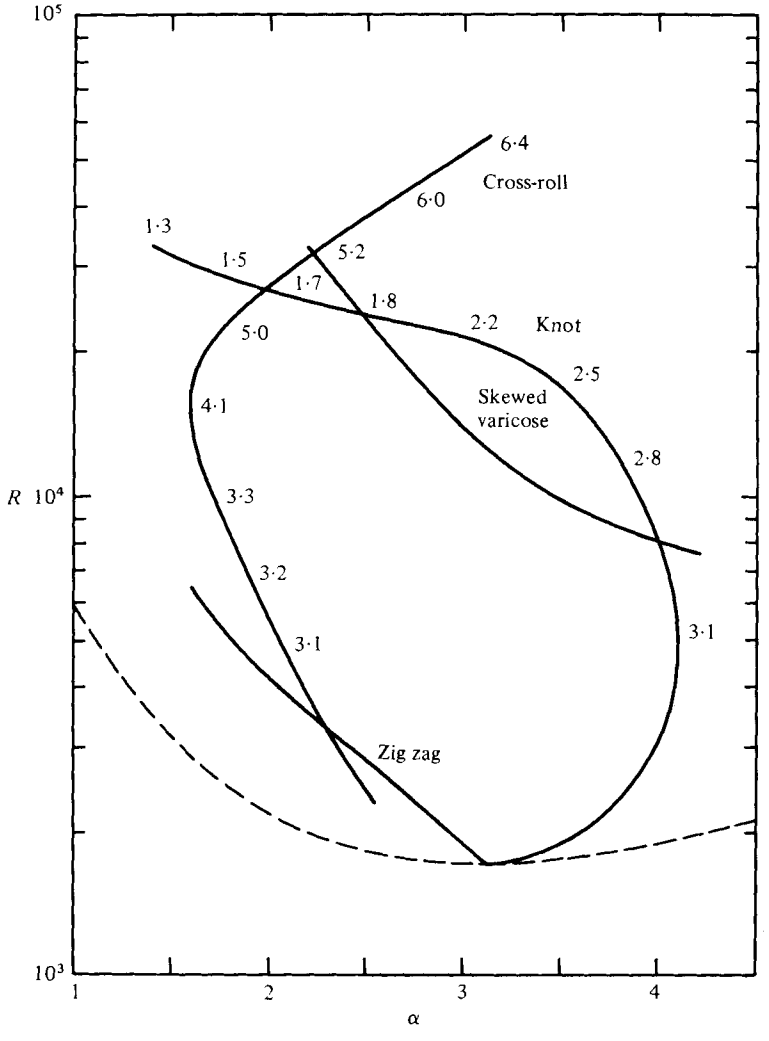


FIGURE 1. Stability diagram for convection rolls for Prandtl number $P = 7{\cdot}0$. Two-dimensional convection with a horizontal wavenumber $\alpha$ is stable in the closed region (below the skewed varicose stability boundary). The numbers refer to the values of $b$. The dashed curve indicates the critical Rayleigh number for the onset of convection.

The stability boundary generated by the knot instability is shown in the case of water in figure 1, and in the case of air in figure 2. The $b$ values of the growing disturbances are given in the figures. On the right-hand side of the figures the knot instability merges smoothly with the ordinary cross-roll instability, while the two instabilities are clearly separated at their crossover point in the upper part of figure 1. The critical Rayleigh number for the onset of the knot instability is shown as a function of the Prandtl number in figure 3 for two different wavenumbers $\alpha$ of the steady rolls. This graph demonstrates that low as well as high Prandtl numbers have a stabilizing effect.

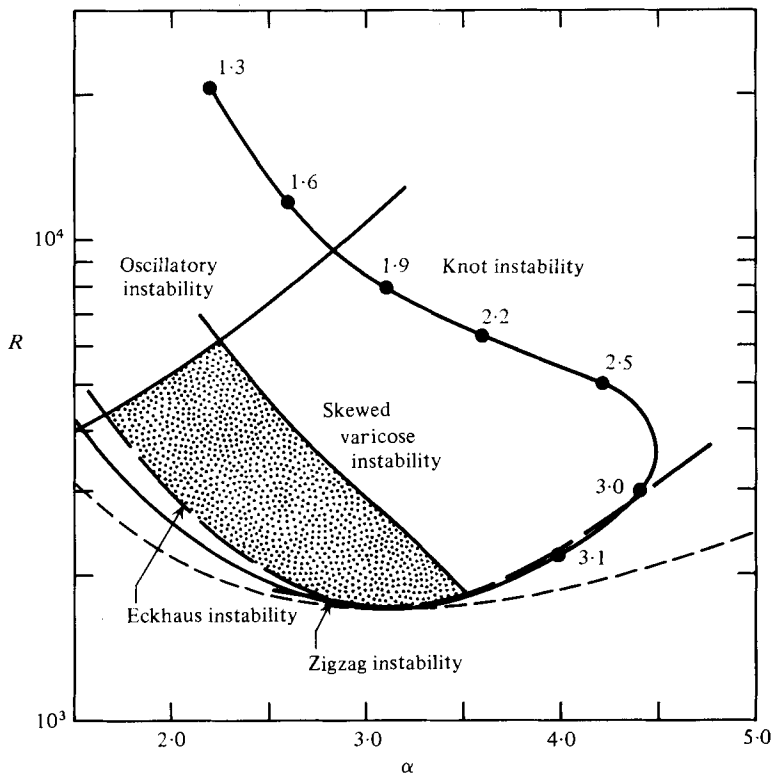


FIGURE 2. Stability diagram for convection rolls in an air layer ($P = 0{\cdot}71$). Two-dimensional convection with a horizontal wavenumber $\alpha$ is stable in the shaded region. The numbers refer to the values of $b$. The dashed curve indicates the critical Rayleigh number for the onset of convection.

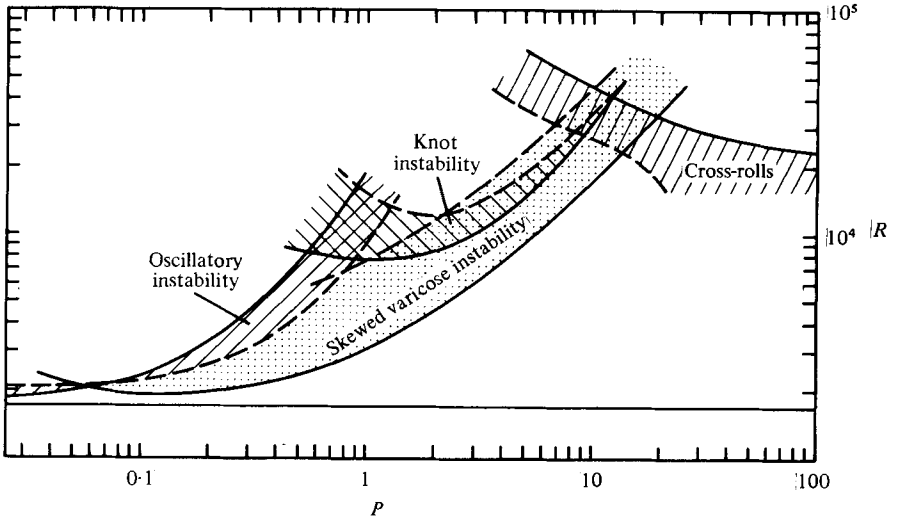


FIGURE 3. Stability boundaries of convection rolls with wavenumbers $\alpha = 3{\cdot}117$ (solid) and $\alpha = 2{\cdot}2$ (dashed) as a function of Rayleigh number $R$ and Prandtl number $P$. Stability boundaries for intermediate wavenumbers lie in the shaded areas.

### 3.3. *The skewed varicose instability*

The skewed varicose instability corresponds to a periodic thickening and thinning of the convection rolls, the phase depending linearly on the $x$ co-ordinate. This latter property causes the characteristic skewed appearance of the disturbed roll pattern. The horizontal dependence of the $y$ velocity of the disturbed convection roll is approximately given by

$$v_y \propto \sin \alpha y + \epsilon \cos[(\alpha+d)\,y + bx] + \epsilon' \cos[(\alpha-d)\,y - bx] + \ldots. \tag{3.1}$$

The disturbance amplitudes $\epsilon$ and $\epsilon'$ become equal in the limit of vanishing $d$. By multiplying the actual solution of the stability equations by a finite factor and adding it to the steady two-dimensional solution, an approximate description of the distorted roll pattern can be obtained. This method has been used to obtain the picture of the vertically averaged temperature distribution shown in figure 4. The factor used in that figure corresponds to the choice $(\epsilon^2+\epsilon'^2)^{\frac{1}{2}} = \frac{1}{2}$ in the truncated series (3.1). The distorted boundaries of the rolls corresponding to the lines of vanishing $v_y$ are indicated by the thick lines. Because of the symmetry of the problem with respect to the $x$ direction the two signs of the skewness are equally possible. Mathematically this corresponds to a change in the sign of $b$. From the general representation (2.3) of the disturbances it is evident that the stability problem does not change when $d$ is replaced by $n\alpha + d$, where $n$ is an arbitrary integer. Within the class of disturbances with even $\lambda+\nu$, $n$ must be an even integer in order that the same stability result is obtained. Since we are considering the skewed varicose instability within the framework of disturbances with even $\lambda+\nu$, we may restrict the discussion to the range $0 \leqslant d < \alpha$.

The critical Rayleigh number $R_{sv}$ for the onset of the skewed varicose instability corresponds to disturbances for which both $b$ and $d$ tend to zero, such that the ratio $d/b$ remains approximately constant at a value close to 1·4. Thus the skewed varicose instability can be considered as a modification of the neutral disturbance

$$\tilde{\phi} = \partial\phi/\partial y, \quad \tilde{\theta} = \partial\theta/\partial y,$$

which is always an exact solution of the stability equations with $\sigma = 0$ and which represents a small translation of the steady roll pattern. The skewed varicose instability shares this property with the zigzag instability and with the oscillatory instability in the case of stress-free boundaries (Busse 1972). As in the case of those instabilities, the growth rate of the critical disturbance remains infinitesimal even when the Rayleigh number exceeds the critical value $R_{sv}$. Only disturbances with finite values of $b$ and $d$ possess finite growth rates. In figure 5 the growth rate $\sigma$ is shown as a function of $d$ for various Rayleigh numbers. In the actual physical situation, the strongest growing disturbance at a given Rayleigh number is most likely to be realized. For this reason the observed values of $b$ and $d$ may vary considerably as a function of $R$. In the case of figure 5, $d$ appears to approach an asymptotic value in the neighbourhood of 1·2. The corresponding value of $b$ is 0·85. The ratio $b/d$ for the strongest growing disturbance changes relatively little as a function of Rayleigh number and Prandtl number, but increases slightly with $\alpha$ from 0·6 at $\alpha = 2{\cdot}2$ to 0·9 at $\alpha = 4{\cdot}6$.

In figure 6 the maximum growth rates $\sigma$ for the skewed varicose and the knot

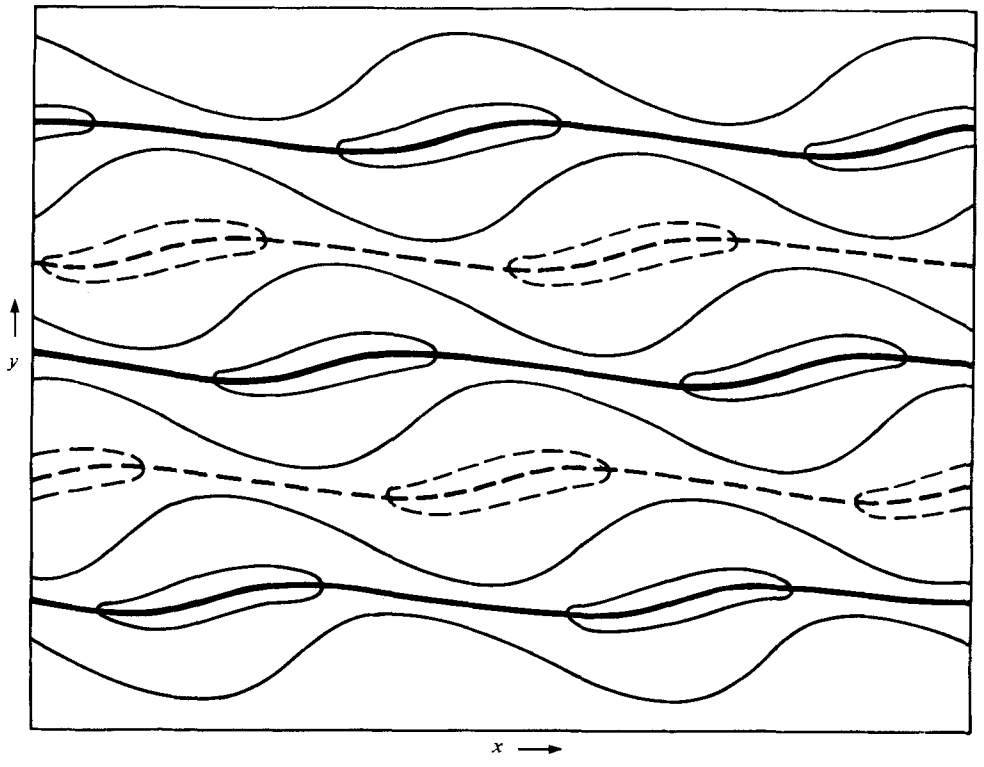


FIGURE 4. Pattern of convection rolls which are distorted by the skewed varicose instability. The thick solid (dashed) lines mark the cell boundary corresponding to hot rising (cold descending) fluid. The thin solid (dashed) lines indicate isotherms of the vertically averaged temperature distribution. The parameters used for the computations are $R = 10^4$, $P = 7$, $\alpha = 3{\cdot}5$, $b = \frac{1}{2}\alpha$, $d = \frac{3}{4}\alpha$.

instability are shown as a function of $R$ for the case $\alpha = 3{\cdot}117$, $P = 7$. The figure demonstrates that the growth rate of the skewed varicose instability increases only quadratically, $\sigma \propto (R - R_{sv})^2$, as the Rayleigh number exceeds the critical value $R_{sv}$. The fact that the growth rates of the two instabilities are comparable at higher Rayleigh numbers is partly responsible for the difficulty of separating them experimentally as is discussed in more detail in § 5.

From figure 4 it is evident that the skewed varicose instability tends to shear and pinch off rolls in such a way that the remaining segments exhibit a larger characteristic wavelength. Indeed, the tendency of the instability mechanism to eliminate large wavenumber rolls in favour of small wavenumber rolls is evident from figures 1 and 2, which show that $R_{sv}$ increases strongly with decreasing $\alpha$, with a resultant shift of the region of stable rolls towards smaller wavenumbers. This property is also borne out in figure 3, where the values of $R_{sv}$ for $\alpha = 2{\cdot}2$ and $\alpha = 3{\cdot}117$ are compared. It

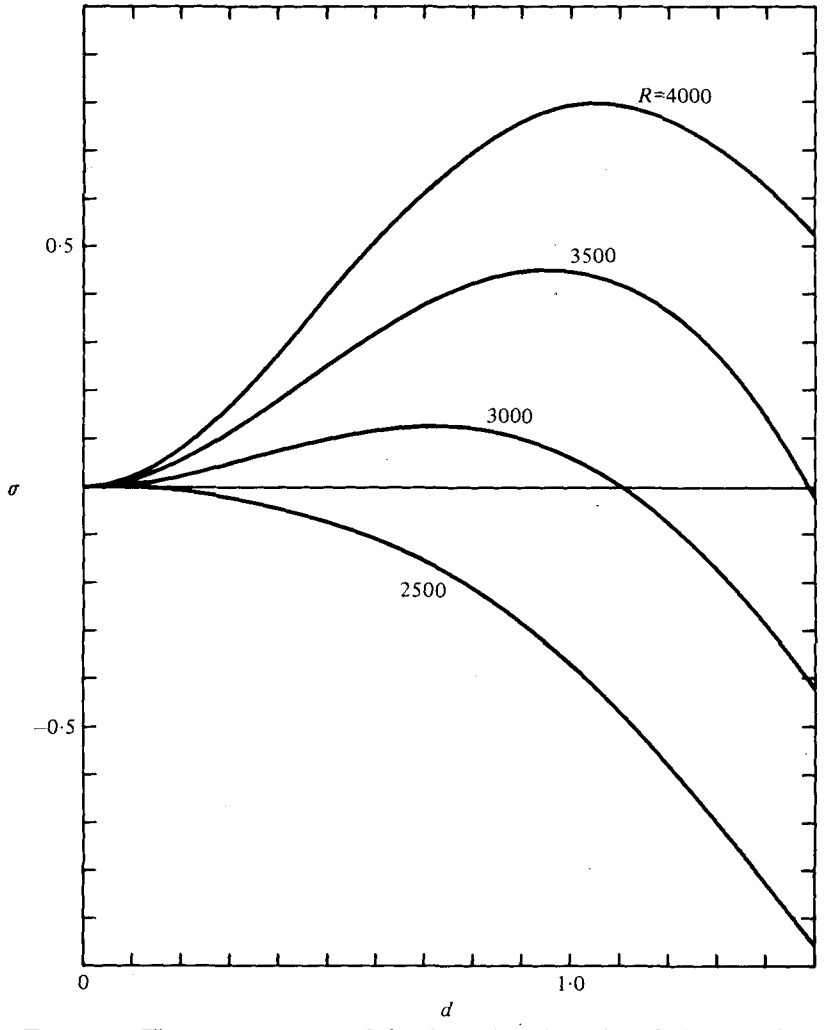


FIGURE 5. The growth rate $\sigma$ of the skewed varicose instability as a function of $d$ for $\alpha = 3{\cdot}117, P = 7{\cdot}0$ and selected values of $R$.

thus appears that the skewed varicose instability plays a major role in the generally observed increase of the average wavelength of convection rolls when the Rayleigh number is increased.

## 4. The experimental method

The experimental apparatus and technique are the same as those described in the papers by Busse & Whitehead (1971, 1974) and only a brief description will be given here. The convection layer consists of a clear liquid sandwiched between two horizontal plate-glass boundaries. Glass plates are also fixed above and below the convection layer in order to create channels through which water of given temperature flows. Because of the finite conductivity of the plate glass, this arrangement fails to provide accurately the condition of a fixed temperature at the boundary of the

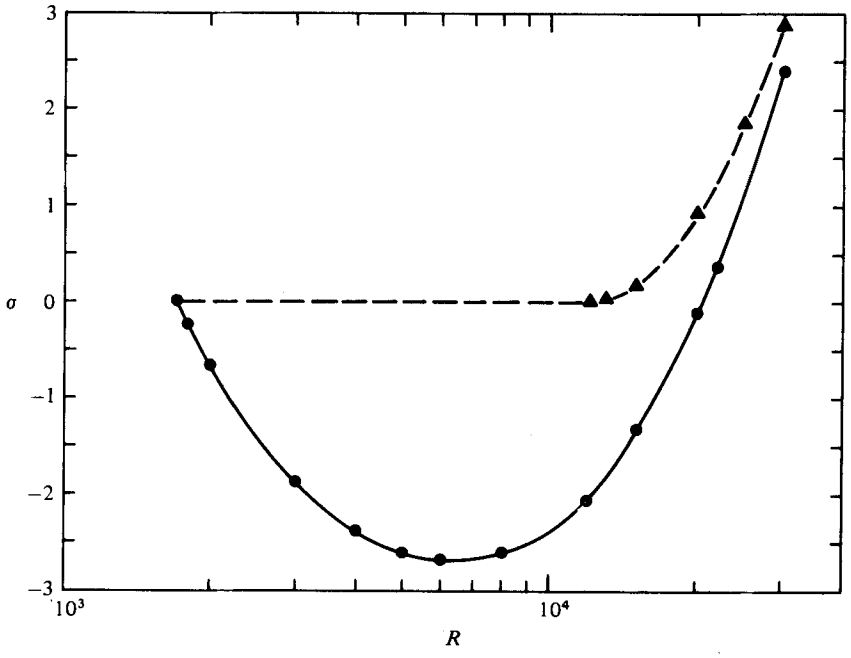


FIGURE 6. The growth rate $\sigma$ of the skewed varicose instability (dashed curve) and for the knot instability (solid curve) as a function of $R$ for $\alpha = 3{\cdot}117$ and $P = 7{\cdot}0$.

convection fluid assumed in the theory. But the use of lucid material has the overriding advantage that the shadowgraph visualization method can be used. The effect of the finitely conducting boundaries is quite noticeable in the experimental results, but it does not seem to influence the qualitative features predicted by theory. Because of the temperature dependence of the refractive index in liquids, hot ascending and cold descending sheets of liquid become visible on a screen in the form of dark and bright lines when a beam of nearly parallel light transverses the layer.

Most convection experiments described in the literature have been done without controlled initial conditions. Accordingly, a rather random pattern of roll-like convection cells is realized when the critical temperature difference is exceeded unless the aspect ratio of the experiment is sufficiently low that the influence of the side walls becomes noticeable in the formation of the pattern. Although there is a tendency towards the development of a more regular roll pattern, this process is hardly ever completed because it is governed by the thermal diffusion time scale based on the horizontal dimension of the convection layer and because it is influenced by very small lateral inhomogeneities. For this reason, controlled initial conditions must be employed to obtain a regular pattern of steady convection rolls. Controlled initial conditions have the additional advantage that the wavenumber $\alpha$ of the rolls can be chosen freely within certain limits.

As in the previous experiments with the apparatus, controlled initial conditions were achieved by placing a grid with the desired wavelength on top of the upper water channel and using a heat lamp to transmit radiative energy through the grid into the convection layer. Although the amount of radiation absorbed by the liquid in the convection layer is small, the resulting spatially periodic temperature rise is

sufficiently large ($\approx 0{\cdot}05$ °K) to dominate over random temperature fluctuations. Except for the somewhat larger amplitude, the effect of the controlled temperature variations on the convection realized does not differ from the effect of the random temperature fluctuations present naturally. The experiment is started by raising the temperature difference between water channels from the nearly isothermal state by proper adjustment of the thermostatic baths and by switching off the heating lamp. The inducement of a regular pattern of rolls of the desired wavelength requires a sufficiently slow rise of the Rayleigh number. An interval of 3–5 thermal diffusion times $h^2/\kappa$ was usually sufficient to achieve a nearly steady state for values of $R$ of the order of $10^4$. Since the corresponding temperature difference $T_2 - T_1$ is of the order of 1 °K, in the absence of convection the initially induced temperature variations would have decayed to less than 1% of the temperature variations caused by convection by the time the steady state was approached and the shadowgraph observations were started.

The steady two-dimensional solution for convection in an infinite layer can only be approximated in a laboratory experiment. Near the side walls the convection flow becomes three-dimensional in general and unsteady processes cause destruction of the initially induced two-dimensional pattern. As time proceeds the disturbances propagate from the side walls towards the interior of the layer and ultimately disrupt the original two-dimensional pattern. The horizontal propagation of the disturbances is basically governed by the velocity of thermal diffusion $\kappa/h$, but it can be significantly faster when the convection pattern is unstable. Because of the large aspect ratio there is usually sufficient time to observe the onset of the instability of the uniform roll pattern. In contrast to the finite amplitude inhomogeneities caused by side-wall effects, the instabilities of the uniform pattern start from nearly infinitesimal disturbances and are characterized by a rather uniform wavenumber $b$. They appear to share all properties of the eigensolutions of the linear stability problem with the exception of the uniform extent over an infinite layer. Because the small disturbances from which the instabilities start are out of phase over distances of the order of $10h$, dislocations similar to those found in crystal lattices are typical. It has never been difficult, however, to distinguish clearly the nearly uniform small amplitude disturbances from the inhomogeneities propagating in from the side walls. In cases when the nearly uniform instability did not develop within a period of about 10 thermal time scales $h^2/\kappa$ the roll pattern was considered as stable with respect to small amplitude disturbances.

The depth $h$ of the convection layer was either 0·55 or 0·84 cm for most experiments. Methyl alcohol and water at different mean temperatures were used as convection fluids. The properties are given in table 1. In order to avoid thermosolutal effects caused apparently by the hygroscopic property of methyl alcohol, this liquid was exchanged frequently. Since the mean temperature difference $\Delta T$ between the boundaries of the convecting fluid is not measured, it must be inferred from the temperature difference $\Delta T_m$ measured between the water channels above and below the convection layer. The formula used for this purpose is

$$\Delta T_m = \Delta T\left(1 + \frac{2k\,d_g}{k_g h} Nu\right), \tag{4.1}$$

where $k_g$ and $d_g$ are the thermal conductivity and thickness of the plate-glass bound-

| | Methyl alcohol (23 °C) | Water (24 °C) | Water (50 °C) |
|---|---|---|---|
| Kinematic viscosity ($10^{-2}$ cm$^2$/s) | 0·710 | 0·916 | 0·562 |
| Thermal conductivity [$10^{-3}$ cal/(cm s °K)] | 0·4767 | 1·444 | 1·528 |
| Thermal diffusivity ($10^{-3}$ cm$^2$/s) | 1·00 | 1·445 | 1·521 |
| Coefficient of expansion ($10^{-3}$ °K$^{-1}$) | 1·24 | 0·246 | 0·455 |
| Prandtl number, $P$ | 7·1 | 6·3 | 3·7 |

TABLE 1. Properties of convection fluids.

aries, and $k$ is the conductivity of the convecting liquid. As in the previous experiments by Busse & Whitehead (1974), the expression $Nu = 0{\cdot}19\,R^{0{\cdot}282}$ was used for the Nusselt number; this appears to give a fair approximation for the experimentally realized value at Rayleigh numbers above $10^4$. Since the wavelength dependence of $Nu$ was not taken into account and because of the uncertainties in the material properties, the absolute values of the Rayleigh numbers used in the experimental results may be in error by as much as 5–10%. The relative accuracy is significantly higher, however.

## 5. Experimental results

The interpretation of the experimental observations in terms of the instability mechanism discussed in the theoretical part of this paper is complicated for a number of reasons. First, the critical values of the Rayleigh number for the onset of the knot and the skewed varicose instability are relatively close for Prandtl numbers larger than 3. There is hardly any suitable liquid available with a smaller Prandtl number, and the experimental technique is not feasible in the case of gases. Second, although the two instability mechanisms are quite distinct from the theoretical point of view, it is not very easy to distinguish them in the shadowgraph observations. The wavenumber $b$ of the strongest growing skewed varicose disturbance is comparable to the expected wavenumber of the knot instability according to figures 1 and 5. Third, the growth rate of the skewed varicose instability is relatively low in the neighbourhood of the critical Rayleigh number $R_{sv}$. Accordingly, the Rayleigh number must be raised appreciably beyond the critical value in order that the growth of the instability becomes visible within an interval of about 10 thermal time scales $h^2/\kappa$, which is usually available before irregular disturbances propagate in from the side walls and destroy the regular pattern. In addition, nonlinear interactions seem to exist by which a finite amplitude skewed varicose disturbance triggers the knot instability and *vice versa*.

It is understandable that the two instabilities have not been distinguished in earlier observations before the theoretical interpretations were available. Actually, neither instability has been clearly observed in the previous observations with the same apparatus at similar Prandtl numbers. Although the patchy process of a varicose-type destruction of the roll pattern reported by Whitehead & Chan (1976) is obviously connected with the skewed varicose instability, it lacked the homogeneity of an instability growing from infinitesimal disturbances. Because of the high conductivity of water and the low heating power of thermostats, a smaller version of the present apparatus was used in the experiments with hot water as the convection fluid described by Whitehead & Chan (1976). The installation of an additional heating element

and the use of methyl alcohol instead of water in the present experiments have resolved this problem and the larger aspect ratio of the present convection layer has provided a more homogeneous condition for the instabilities.

A good example of the occurrence of the skewed varicose instability is shown in figure 7 (plate 1). The instability starts with a small wavy distortion (figure 7*b*) of the originally uniform roll pattern (figure 7*a*). As the disturbance grows (figure 7*c*), it tends to pinch the rolls (figure 7*d*) and to form cells in the form of short rolls with nearly twice the wavelength of the original rolls (figure 7*e*). At the time of figure 7(*f*), the establishment of rolls with larger wavelength than the original ones is clearly evident even though the pattern continues to change in time at a slower rate. Thus the skewed varicose instability does not correspond to a transition to a qualitatively new kind of convection pattern, but instead transforms the roll pattern into another one with a stable wavenumber. The increase of the characteristic wavelength of convection caused by the skewed varicose instability is even more pronounced at lower Prandtl numbers, as the stability graph for air shown in figure 2 indicates. This agrees with the general experimental observation (Willis, Deardorff & Somerville 1972) that the characteristic wavelength at finite amplitude of convection increases with decreasing Prandtl number even though $\alpha_c$ is independent of the Prandtl number. The observation made by Busse & Whitehead (1971) that larger rolls always grow at the expense of smaller rolls when both are joined by a pinch is also in accordance with this property of the skewed varicose instability.

In contrast to the skewed varicose instability, the knot instability leads to a new form of convection, namely spoke-pattern convection. The knot instability is essentially identical to the collective instability which produces the transition from bimodal or oscillatory bimodal convection to spoke-pattern convection, and which was described in detail by Busse & Whitehead (1974). Figure 8 (plate 2) shows that the transition to bimodal convection owing to the cross-roll instability, corresponding to the high $b$ wavenumber disturbances in the photographs and the transition to spoke-pattern convection owing to the knot instability, corresponding to the low $b$ wavenumber disturbances, may take place almost at the same time. This phenomenon is even more pronounced in figure 9 (plate 3), where the transition to bimodal convection appears to occur initially. The cross-roll instability, producing bimodal convection, has usually larger growth rates, but it is always ultimately superseded by the knot instability in the region where both may occur. On the other hand, the regular spoke pattern figures (8*f* and 9*d*) resulting from the knot instability remains stable only when the wavelength of the basic rolls is rather large. Otherwise the skewed varicose instability modifies the spoke pattern. Thus the experimental observations indicate that the various instabilities of two-dimensional convection rolls continue to operate in those regions where the rolls have already been replaced by a three-dimensional form of convection. At relatively large values of $\alpha$, the knot instability does not differ much from the ordinary cross-roll instability, which limits the stability region of rolls towards high wavenumbers $\alpha$. Figure 10 (plate 4) shows this close relationship, which must be expected on theoretical grounds since the knot instability represents a particular branch of the cross-roll instability. Some influence of the skewed varicose instability mechanism is also noticeable in figure 10(*c*), with the typical consequence of large wavelength rolls visible in figure 10(*d*).

A quantitative display of the observational data is given in figure 11. Only the

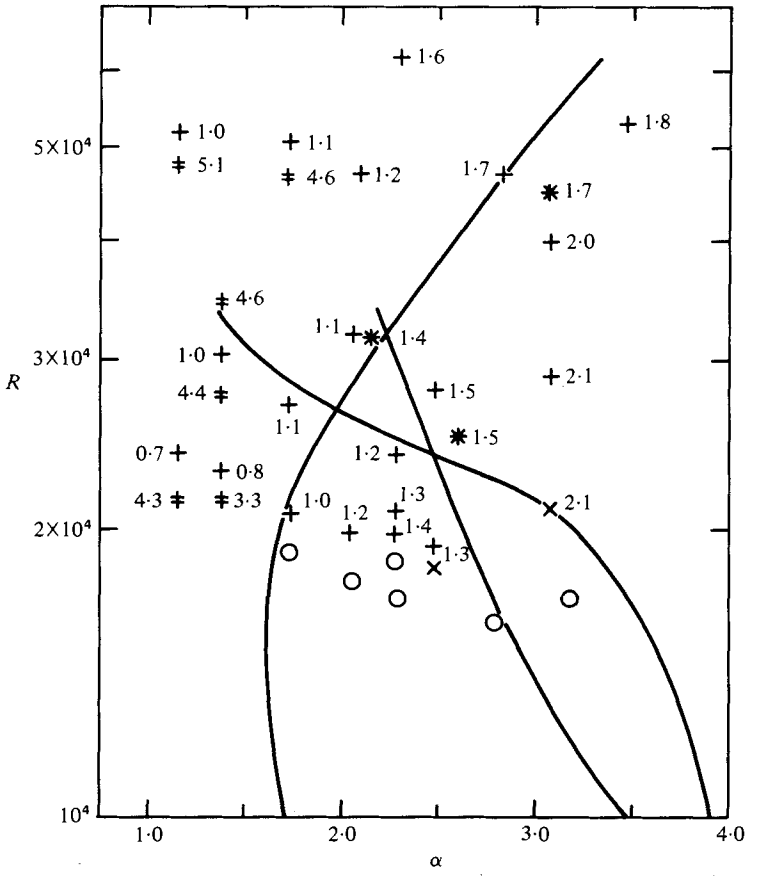


FIGURE 11. Experimental observations of instabilities of convection rolls in methyl alcohol in comparison with the critical stability boundaries (see figure 1). ǂ, cross-roll instability; +, knot instability; ×, skewed varicose instability; ✱, cases where it is not possible to distinguish the dominant instability between the latter two. The numbers refer to the observed wavenumber $b$.

observations for methyl alcohol are shown since this liquid approximates better than water the theoretical assumption of an infinite ratio between the conductivities of the boundary and the convecting fluid. The finite conductivity of the methyl alcohol is evidently responsible for the shift of the experimentally observed stability boundaries towards lower wavenumbers and lower Rayleigh numbers as must be expected because of the less constraining boundary condition for the temperature. The observed wavenumber $b$ of the instability also exhibits this effect, which was found earlier in the case of higher Prandtl numbers (Busse & Whitehead 1971). In the present investigation, attention has been focused on the upper part of the stability diagram for rolls because of the new instabilities occurring in this regime. The cross-roll instability and the zigzag instability, which dominate in the lower part of the theoretical stability chart of figure 1, have been investigated in the earlier experiments by Busse & Whitehead (1971) and Whitehead & Chan (1976).

The experimental observations with water agree qualitatively with those in the case of methyl alcohol. Because of the higher conductivity of water, the observed

stability boundary is shifted even more towards lower wavenumbers than is shown in figure 11. Because of the lower Prandtl number of hot water, the knot and the skewed varicose instabilities occur at lower Rayleigh numbers, in agreement with the theory.

## 6. Discussion

The finite amplitude properties of thermal convection are governed by two nonlinear terms in the basic Boussinesq equations. These terms describe the advection of momentum and of heat. The Prandtl number provides a measure of the relative importance of these terms in the sense that the advection of momentum becomes dominant for small values of $P$, but vanishes in the limit $P \to \infty$. The original expectation was that the stability properties of convection at a finite Prandtl number could be understood in terms of the mechanisms of instability present in the limiting cases of small and large Prandtl number. The results of this paper describe a more complicated picture since both the knot instability and the skewed varicose instability disappear for large as well as small Prandtl numbers.

Although the Prandtl number dependence provides important clues in the understanding of instability mechanisms in general, it does not provide much insight in the case of the knot and skewed varicose instabilities. These instabilities obviously depend on an interaction of the advection of momentum and of heat, but the details of this interaction are not easily accessible in the numerical approach used in this paper. Since the stability boundary of the skewed varicose instability approaches the curve $R_c(\alpha)$ which describes the Rayleigh number for the onset of convection of a given wavenumber $\alpha$, an analytical theory based on a small amplitude perturbation theory should be possible. But this has not yet been attempted.

Since it is impossible to obtain computational results for all possible values of the parameters of the stability theory, the possibility of an instability corresponding to a steep rise of the growth rate in a narrow region of the parameter space cannot easily be dismissed. Although no indication of such a behaviour has ever been found, the confirmation of the theoretical results by the experimental observations is reassuring. The fact that all transitions predicted by the linear stability theory can actually be observed is unusual since subcritical finite amplitude instabilities occur in many hydrodynamic systems. Within the experimental accuracy, this phenomenon can be excluded for the cases investigated in this paper.

Besides confirming the theoretical results in all qualitative aspects, the experimental observations provide important information beyond the scope of the stability theory. The instabilities predicted for the roll solution appear to occur with little modification even after the convection rolls have already experienced a transition to a three-dimensional pattern. The mechanisms of higher transitions can thus be understood in terms of the instabilities of two-dimensional rolls. The explanation of the collective instability of bimodal convection (Busse & Whitehead 1974) in terms of the knot instability is a typical example. Indeed, there appears to be no observed instability in the Rayleigh number range up to a few times $10^5$ which is not related to one of the known instabilities of two-dimensional rolls. It must be said, though, that it becomes increasingly difficult at high Rayleigh numbers to generate regular three-dimensional patterns of convection and to observe their instabilities. In parti-

cular, more careful observations of spoke-pattern convection are needed to learn about further instability mechanisms involved in the development towards fully turbulent convection.

The support of the research reported in this paper by the Atmospheric Section of the U.S. National Science Foundation under Grant Atm 76-22280 is gratefully acknowledged. A major portion of the computations was made possible through funds supplied by the Campus Computing Network at UCLA.

## REFERENCES

BUSSE, F. H. 1967 On the stability of two-dimensional convection in a layer heated from below. *J. Math. & Phys.* **46**, 140–150.

BUSSE, F. H. 1972 The oscillatory instability of convection rolls in a low Prandtl number fluid. *J. Fluid Mech.* **52**, 97–112.

BUSSE, F. H. & WHITEHEAD, J. A. 1971 Instabilities of convection rolls in a high Prandtl number fluid. *J. Fluid Mech.* **47**, 305–320.

BUSSE, F. H. & WHITEHEAD, J. A. 1974 Oscillatory and collective instabilities in large Prandtl number convection. *J. Fluid Mech.* **60**, 67–79.

CHANDRASEKHAR, S. 1961 *Hydrodynamic and Hydromagnetic Stability*. Oxford: Clarendon Press.

CHEN, M. M. & WHITEHEAD, J. A. 1968 Evolution of two-dimensional periodic Rayleigh convection cells of arbitrary wavenumbers. *J. Fluid Mech.* **31**, 1–15.

CLEVER, R. M. & BUSSE, F. H. 1974 Transition to time-dependent convection. *J. Fluid Mech.* **65**, 625–645.

MOIR, G. 1976 The stability of finite amplitude Bénard convection. Ph.D. thesis, Newcastle-upon-Tyne Polytechnic.

WHITEHEAD, J. A. & CHAN, G. L. 1976 Stability of Rayleigh–Bénard convection rolls and bimodal flow at moderate Prandtl number. *Dyn. Atmos. Oceans* **1**, 33–49.

WILLIS, G. E., DEARDORFF, J. W. & SOMERVILLE, R. C. 1972 Roll-diameter dependence in Rayleigh convection and its effect upon the heat flux. *J. Fluid Mech.* **54**, 351–367.

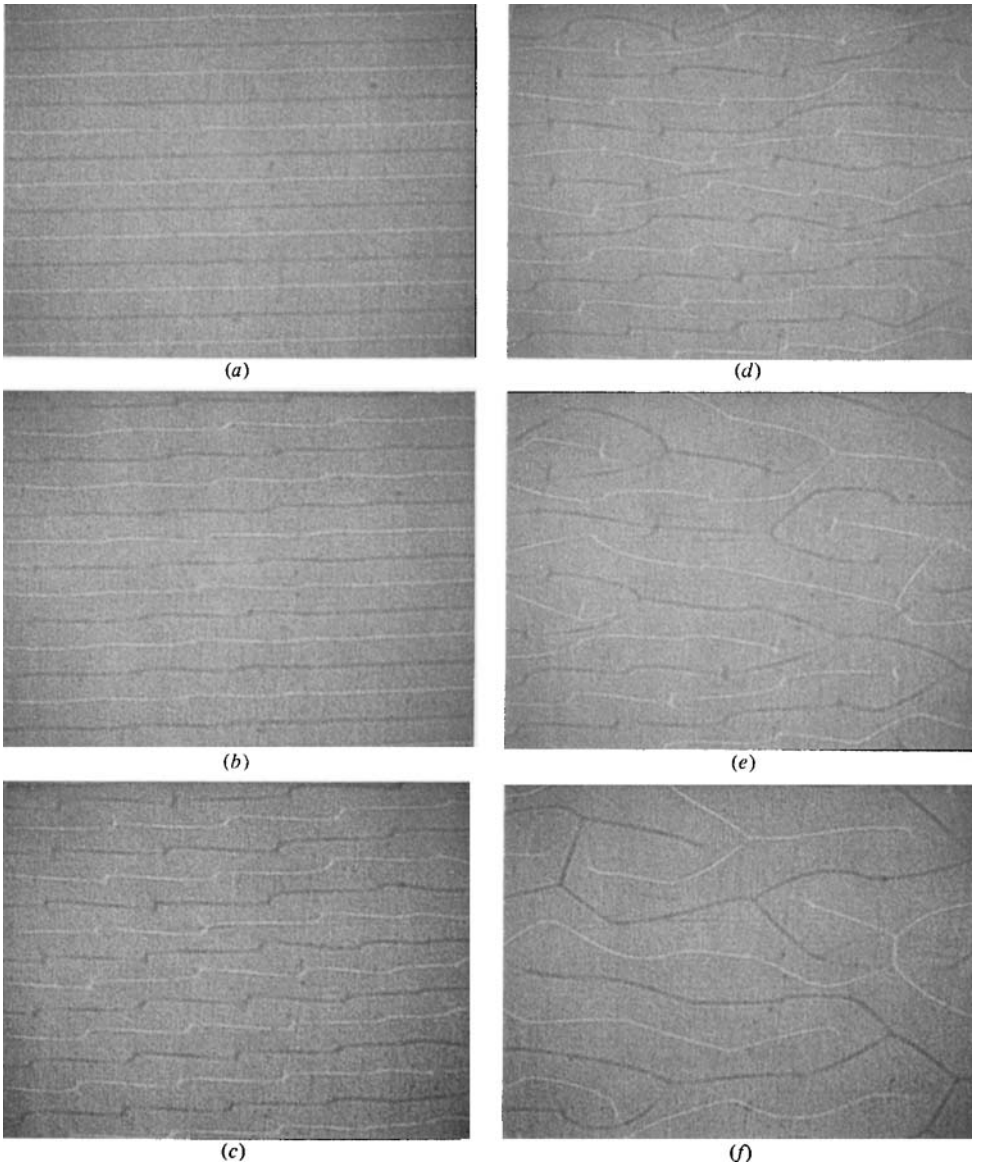


FIGURE 7. The onset of the skewed varicose instability in water with a mean temperature of 50 °C, $h = 5{\cdot}5$ mm and $\alpha = 1{\cdot}38$. The Rayleigh number $R$ increases slightly from $10^4$ to $1{\cdot}1 \times 10^4$. The time intervals between subsequent pictures are 4, 5, 3, 4 and 8 min, respectively.

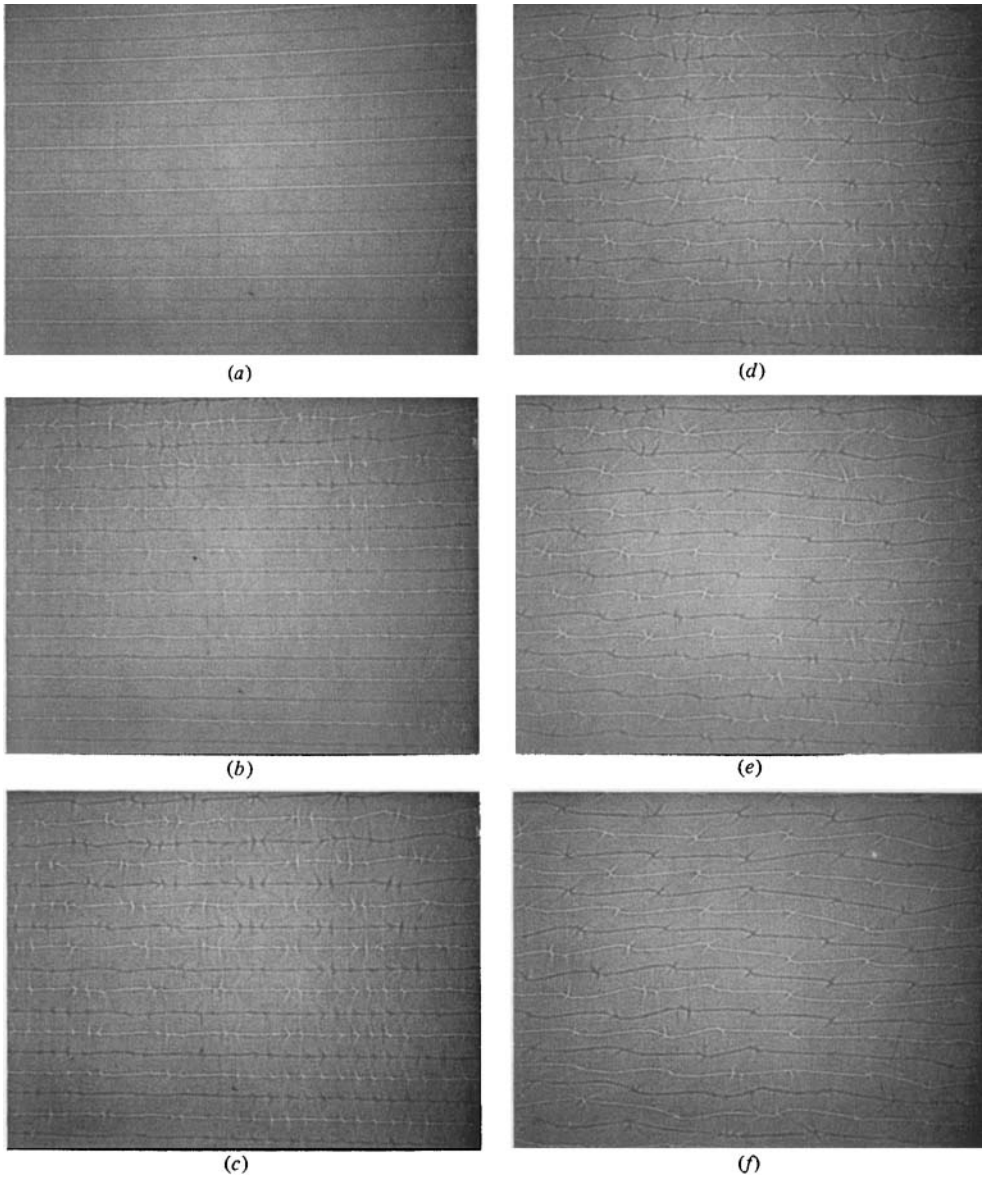


FIGURE 8. The onset of the knot instability in methyl alcohol with $h = 8{\cdot}4$ mm, $\alpha = 1{\cdot}74$. $R$ increases slightly from $4{\cdot}5 \times 10^4$ to $5{\cdot}5 \times 10^4$. The time intervals between subsequent pictures are 6, 2, 3, 2 and 6 min, respectively.

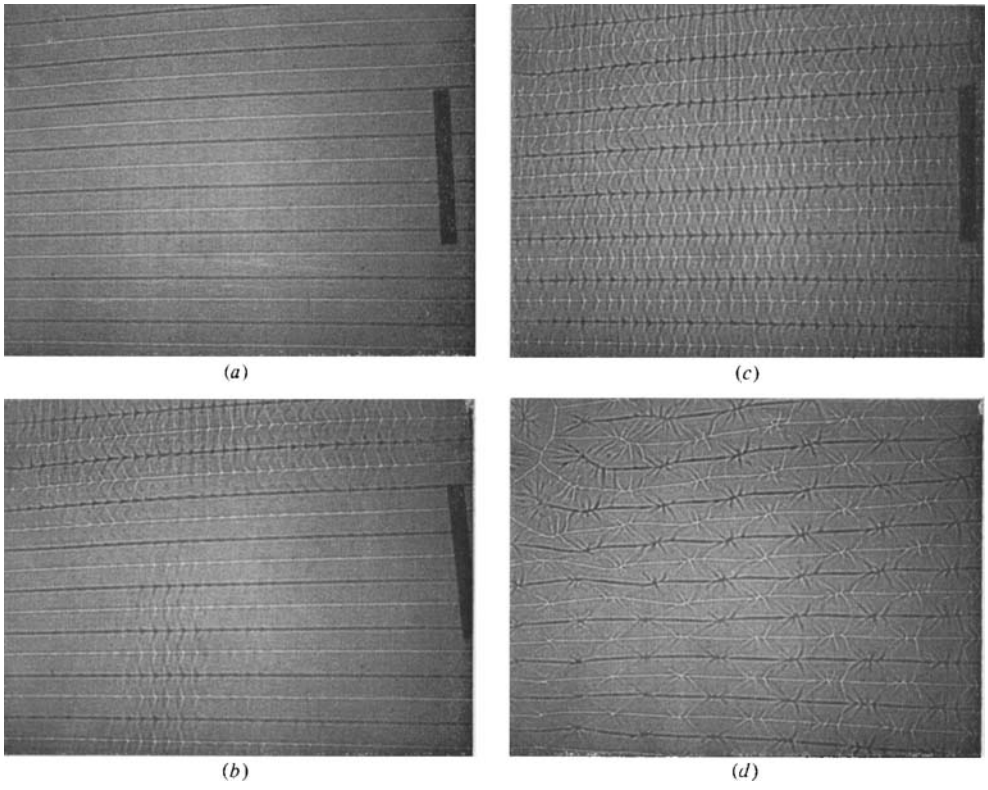


FIGURE 9. The joint onset of the cross-roll and the knot instabilities in methyl alcohol with $h = 5{\cdot}5$ mm, $\alpha = 1{\cdot}2$. $R$ increases from $2{\cdot}8 \times 10^4$ to $3{\cdot}6 \times 10^4$ and the time intervals between subsequent pictures are 2, 1 and 11 min, respectively.

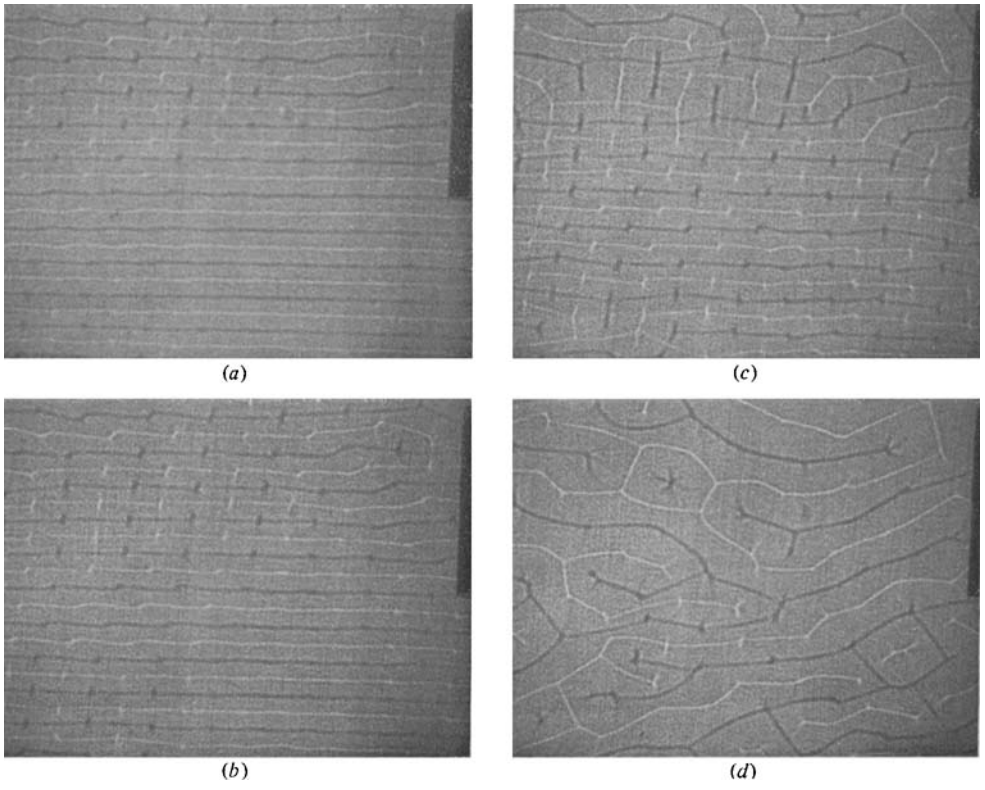


FIGURE 10. The onset of the knot instability in water with a mean temperature of 24 °C, $h = 5{\cdot}5$ mm, and $\alpha = 2{\cdot}05$. $R$ increases slightly from $10^4$ to $1{\cdot}1 \times 10^4$. The time interval between subsequent pictures is 2 min.